

A dielectrophoretic barrier-based microsystem for separation of microparticles

Dafeng Chen · Hejun Du

Received: 13 October 2006 / Accepted: 28 December 2006 / Published online: 8 February 2007
© Springer-Verlag 2007

Abstract This paper presents a microfluidic system for separation of microparticles based on the use of dielectrophoretic barriers, which are constructed by aligning two layers of microelectrode structure face-to-face on the top and bottom sides of the microchannel. The energized barriers tend to prevent the particles in the flow from passing through. However, particles may penetrate the barriers if a sufficiently high flow rate is used. The flow velocity at which the particles begin to penetrate the barrier is defined as threshold velocity. Different particles are of different threshold velocities so that they can be separated. In this paper, the electrodes are configured with open ends and aligned with a certain angle to the direction of the flow. Polystyrene microbeads of different sizes (i.e., 9.6 and 16 μm in diameter) are studied in the tests. Under the experimental conditions, two particle trajectories are observed: the 9.6 μm beads penetrate the barriers and move straightly toward the fluidic outlet, while the 16 μm beads snake their way along the electrode edges at a relatively low speed. The two subpopulations of particles are separated into spatial distance of ~ 10 mm within tens of seconds. The system presents a rapid and dynamic separation process within a continuous flow.

Keywords Dielectrophoresis · DEP barrier · Particle separation

1 Introduction

One of the major steps in most of the biomedical operations consists of concentrating and separating the analytes such as cells of interest from the background matrix and positioning them into selected locations for subsequent treatments and analysis. The use of alternating current (AC) electric field has been demonstrated to be of great potential for such applications. It has been shown that dielectrophoresis (DEP), which arises from the interaction of nonuniform AC electric field with the induced dipole in the particle (Jones 1995), can be used for the analysis and separation of a variety of microscopic particles, particularly biological particles such as cells (Pethig 1996), viruses (Hughes et al. 1998), and DNA (Washizu et al. 1995). Depending on the dielectric properties of the particles and medium, particles are either attracted to regions of high field strength (i.e., positive DEP) or repelled away from them (i.e., negative DEP) (Pohl 1978). A dielectrophoretic microsystem generally consists of a microchannel equipped with an array of electrodes capable of generating a high gradient electric field that drives the analytes to move. The available miniaturization technology allows the integration of these components into a single microchip. A variety of microelectrode designs have been proposed, including planar electrodes such as interdigitated electrode array (Li and Bashir 2002; Chen et al. 2005), polynomial electrode (Huang and Pethig 1991), castellated electrode (Pethig et al. 1992), and three-dimensional cage design (Schnelle et al. 2000).

A DEP continuous microparticle sorting system based on planar electrodes has been proposed by Kralj et al. (2006). The sorting system based on planar

D. Chen (✉) · H. Du
School of Mechanical and Aerospace Engineering,
Nanyang Technological University,
Singapore, Singapore 639798
e-mail: dfchen@ntu.edu.sg

H. Du
e-mail: mhdu@ntu.edu.sg

electrodes were simple and easy to fabricate, but might suffer from problems such as nonuniform flow and nonspecific particle adhesion at the top walls. This paper presents a dielectrophoretic system for continuous separation of microparticles based on the use of a three-dimensional electrode structure—the paired electrode array or barrier (Schnelle et al. 1999; Dürr et al. 2003; Chen et al. 2006). The 3D microelectrode array is constructed by aligning two layers of electrodes face-to-face on the bottom and top sides of a channel. The array contains more than 30 pairs of electrodes and covers a length of ~ 10 mm of the channel. Dielectrophoretic barriers are formed by applying high-frequency AC voltages on the electrode pairs. The particles running along with the flow will exhibit two types of movements: penetrating the barrier or moving along the electrode edges, depending on the relative strength of the DEP force and hydrodynamics force on the particles. With a proper flow rate, particles of different dielectric properties or/and sizes can be readily separated. In this paper, the separation of the particles is achieved by taking advantages of their differences in traveling velocities in the flow under the effects of the DEP and hydrodynamic forces. Latex beads of diameters of 9.6 and 16 μm , respectively, are investigated in the tests. The beads are spatially separated in the channel, and reached the outlet in a time interval of minutes. Typically, the two subpopulations of particles are separated into spatial distance of ~ 10 mm within tens of seconds using the present microsystem.

2 Theory and methodology

The paired electrode system is schematically shown in Fig. 1. Two layers of electrodes are placed face-to-face on the bottom and top sides of the channel (Fig. 1a). The electrodes are aligned at an angle of θ with reference to the channel wall (Fig. 1b). The flow is running from the left to the right and AC voltage is applied to the electrodes via the contact pads. Particles traveling in the flow will be subjected to the DEP force as well as the hydrodynamic force. In terms of negative

DEP where the particle is less polarizable than the suspending medium, the DEP force tends to push the particles away in the vicinity of the electrodes, while the hydrodynamic force drags the particles along the flow. These two force components are simultaneously acting on the particles and competing against each other. The resulting particle movement, i.e., penetrating the DEP barrier or being deflected there, is determined by the relative strengths of the forces. As shown in Fig. 1b, the particle will penetrate the DEP barrier as long as $F_{HD\perp} \geq F_{DEP}$. The flow velocity at which the particle begins to penetrate the DEP barrier is defined as threshold velocity, which is given by solving the equation $F_{HD\perp} \geq F_{DEP}$. The threshold velocity is (Chen et al. 2006)

$$V_{th} = \frac{F_{DEP}}{6\pi\eta a \sin \theta}, \quad (1)$$

where η is the viscosity of the fluid, a is the particle radius. The DEP force F_{DEP} is given by (Jones 1995)

$$F_{DEP} = 2\pi\epsilon_0\epsilon_m a^3 \text{Re}(f_{cm}) \nabla E^2, \quad (2)$$

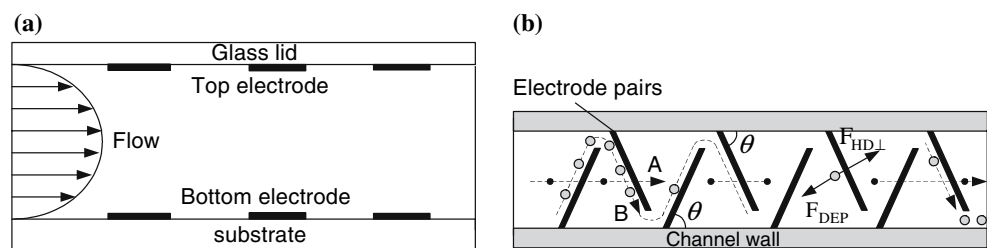
where $\epsilon_0 = 8.854 \times 10^{-12} \text{Fm}^{-1}$ is the permittivity of free space, ϵ_m is the relative permittivity of the surrounding medium, E is the rms (root-mean-square) value of the electric field, and f_{cm} is the Clausius–Mossotti factor, a complex function of the medium and particle complex permittivities, given by

$$f_{cm} = \frac{\epsilon_p^* - \epsilon_m^*}{\epsilon_p^* + 2\epsilon_m^*} \quad (3)$$

with $\epsilon^* = \epsilon - i\sigma/\omega$; ω is the frequency of the applied voltage. Subscripts p and m denote particle and suspending medium, respectively.

Equation 1 implies that the threshold velocity depends on parameters including the DEP force, fluid viscosity η particles size a , and the aligning angle θ of the electrode. At the velocity, which is higher than V_{th} , particles will penetrate the barrier and move along with the flow. Different particles are of different threshold velocities, and therefore they can be separated.

Fig. 1 Schematic diagram of the paired electrode system. **a** Cross section view. **b** Top view. The two possible movements of the particles are shown in **b** as indicated by dotted lines with ‘A’ and ‘B’



rated by adjusting the flow rate. The threshold velocities for two micrometer-sized beads of diameters of 9.6 and 16 μm , respectively, are numerically calculated (Chen et al. 2006), as shown in Fig. 2. In the calculation, the aligning angle is 45° and frequency of applied voltages is 100 kHz. The whole domain of the graph is divided into three functional regions, as indicated by sequence numbers (I)–(III). These three regions are:

- I. Region of accumulation: A flow velocity lower than both the threshold velocities of the two particles is used. In such a flow, the DEP force is dominant and both the particles cannot pass through the dielectrophoretic barrier, resulting in accumulation of the particles.
- II. Region of separation: A flow velocity between the threshold velocities of the two particles results in separation of the particles. The particle of smaller size penetrates the dielectrophoretic barrier while the other settles by the gate.
- III. Wash-away region: velocities higher than both the threshold velocities of the particles will wash away all the particles. The dielectrophoretic barrier fails to deflect the particles. This is useful in collecting the accumulated or separated particles.

The working principle of separating the microparticles with the paired microelectrode system is schematically shown in Fig. 1b. With a flow rate within region (II), the two different particles running from left to right will follow the paths A and B, respectively. One will penetrate the dielectrophoretic barriers and run all the way to the exit of the channel (path A), while the other will be deflected by the barriers and snake its way along the electrodes (path B). They are able to be spatially

separated because of their differences in the traveling velocities and the distance needed to travel from the inlet to the outlet of the channel. If the velocity of flow (in the channel centerline where the particles are levitated) is V_0 , the velocities of the particles along the two paths are $V_A = V_0$ and $V_B = V_0 \cos \theta$, respectively. Note that the traveling velocity along path B is assumed to be constant in obtaining the above equations even when the particle is passing through the electrode pairs. This assumption is reasonable when microelectrodes are used. The distances they need to travel are $l_A = L$ and $l_B = L / \cos \theta$, respectively, with L being the length of the channel. Because of this, the two different particles will reach the outlet at a different time. The time interval between the particles is denoted as

$$\Delta t = L/V_0(1/ \cos^2 \theta - 1). \tag{4}$$

Equation 4 indicates that Δt is dependent on parameters including the length of the channel (but not the width of the channel), the flow rate, and the aligning angle of the electrode pairs. For example, taking the following values for the channel length and flow rate: $L = 20 \text{ mm}$, $V_0 = 500 \mu\text{m/s}$, the time interval Δt calculated from the above equation are shown in Fig. 3 for various aligning angles. It can be seen that Δt increases rapidly as the aligning angle increases. Furthermore, the time interval can range from tens of seconds to $\sim 10 \text{ min}$, which is sufficient for the subsequent operations such as collection of the separated subpopulations at the outlet of the channel. This suggests useful ideas for designing the electrode structures for the separation of particles. A large aligning angle will be of advantage, but on the other hand it reduces

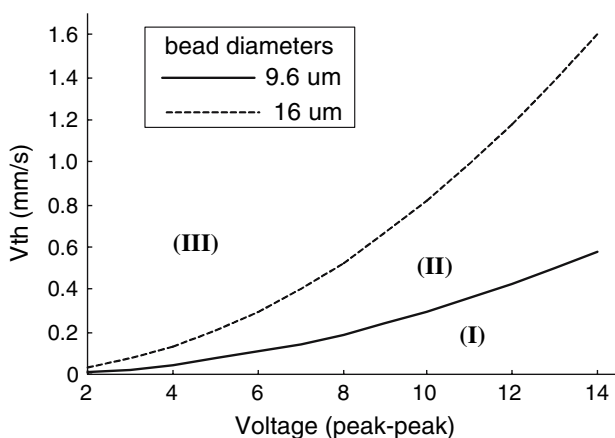


Fig. 2 The threshold velocities as a function of applied voltage for two latex beads of diameters of 9.6 and 16 μm , respectively. Aligning angle is 45° and frequency $f = 100 \text{ kHz}$

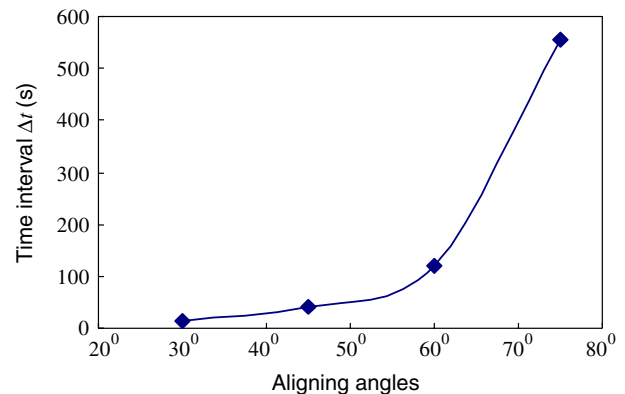


Fig. 3 The time interval Δt for various aligning angles. In the calculation, $L = 20 \text{ mm}$, $V_0 = 500 \mu\text{m/s}$

the range of working flow rates by reducing the threshold velocity (Eq. 1). A compromise between them should be made for the practical applications.

3 Materials and microfabrication

3.1 Particle suspension

Suspensions of microparticles used in the experiments were made by re-suspending the polystyrene beads (cross-linked with 4–8% divinylbenzene DVB, Duke Scientific Co., Palo Alto, CA, USA) in de-ionized water at low concentration. The beads of diameters of 9.6 and 16 μm , respectively, were mixed with a ratio of 1:1. Conductivity of the suspension was adjusted by adding phosphate buffer solution (PBS, Fisher Scientific, Springfield, NJ, USA) into the suspension. The conductivity was measured using a conductivity meter with graphite sensor electrodes (Dist3WP, Hanna Instruments Inc., Woonsocket, RI, USA). Medium conductivity of 10.0 mS/m was used in the tests.

3.2 Microfabrication

The microfabrication process is similar to that in (Chen et al. 2006). The process involved two wafers on which parallel fabrication steps were performed (Fig. 4). The two wafers, i.e., a 4-in. glass wafer (Pyrex 7740) and a silicon wafer with 1 μm silicon dioxide (SiO_2) thermally grown on the surface as the insulation layer, were cleaned in Piranha solution for 20 min before

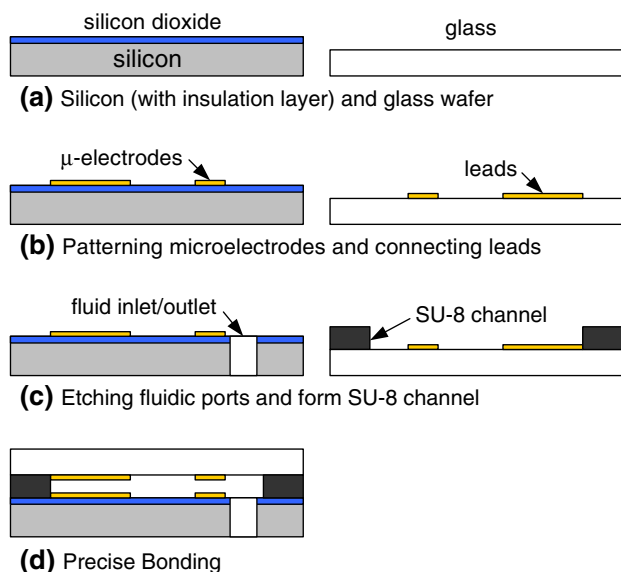


Fig. 4 Microfabrication process of the paired microelectrode DEP system for particle separation

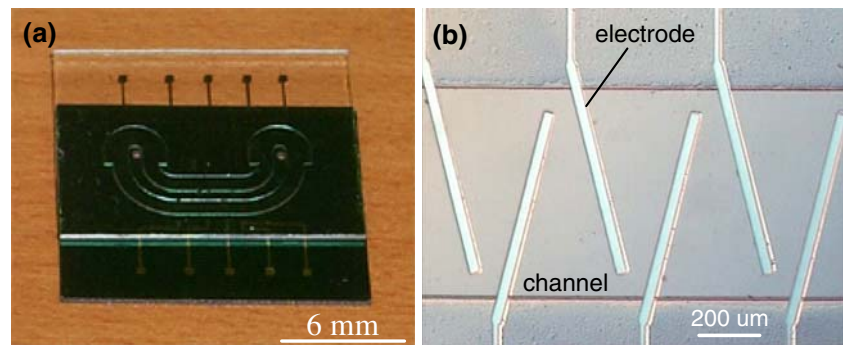
photolithography. The electrode layer of 25 nm Cr/100 nm Au was deposited using magnetron sputtering process, and patterned with acetone lift-off technique. An ultrasonic source was used to expedite the resist stripping process during lift-off process. The silicon wafer coated with microelectrodes on the surface was then etched through using Inductively Coupled Plasma (ICP) deep reactive ion etching to fabricate the fluidic inlet and outlet of diameter of 600 μm . A 10- μm layer of AZ 9260 (Clariant, Charlotte, NC, USA) resist was used as mask during the etching. Meanwhile, a micro-channel of 75 μm in height, 800 μm in width was constructed with the epoxy-based photosensitive resist SU-8. At this point, the wafers were ready for bonding. For this purpose, alignment marks were defined on the two wafers in the prior microelectrode fabrication step. The electrode face-to-face alignment was performed at wafer level using a mask aligner (Karl Suss MA6) and found to be of micrometer precision. A two-part epoxy-based adhesive (Araldite Rapid, Huntsman Advanced Materials (UK) Ltd., Cambridge, UK) with 5-min curing time was applied on the surface of developed SU-8 layer by a lamination process. The adhesive provided a bond of good coverage, high bonding strength, and small adhesive thickness. Typical thickness of the adhesive layer less than 1 μm was determined by microscopic examination of the cross section of a sample.

A completed DEP chip fabricated with the above process is shown in Fig. 5a. Two diced slides containing planar electrode arrays were bonded together with electrode precisely aligned facing each other. The contact pads were left uncovered for wire bonding to the electrical connection on the PCB. The fluidic ports, i.e., fluid inlet and outlet, were located at the ends of the channel. Fig. 5b shows part of the paired microelectrode array and the channel.

3.3 Experimental setup

Sine wave excitation up to 20 MHz and 15 $V_{\text{pk-pk}}$ (into 50 Ω) was generated by a Wavetek 90 Function Generator (Wavetek Wandel and Goltermann Inc., Raleigh, NC, USA). The electrical output was connected to the contact pads at the edge of the substrate via a customer-made PCB. The electrical on/off status of each electrode was separately controlled by the multi-way switches on the PCB. Fluidic connection to the package was made via fitting and silicone tubing (Cole-Parmer In. Co., Chicago, IL, USA). A syringe pump (Model NE-1000, New Era Pump System Inc., New York, NY, USA) was used for precise control of the buffer and particle stream at a flow rate of 10–500 $\mu\text{l/h}$,

Fig. 5 **a** The DEP chip fabricated with the process in Fig. 4 containing the paired microelectrode array, connection leads and pads, microchannel, and fluidic ports. **b** The microfabricated paired electrode array and the channel



in combination with a four-way valve (V-101D, Upchurch Scientific, Oak Harbor, WA, USA). A microscope system Olympus MX40 mounted with CCD and Video camera was used for inspection of the particle movements.

4 Results and discussion

4.1 Particle trajectory

Polystyrene beads of 9.6 and 16 μm in diameter were used in the test. As discussed in Sect. 2, a flow rate between the threshold velocities of the two particles will result in the separation of the particles. The trajectory of the particles is shown in Fig. 6. The aligning angle of the electrodes was 75° and the applied voltage was set at $15 V_{pk-pk}$ at a frequency of 1 MHz. A flow of

90 $\mu\text{l/h}$ (mean flow velocity was $\sim 400 \mu\text{m/s}$) as applied from the left to the right by the syringe pump. Two types of particle movements were observed in the vicinity of electrode pairs. The 9.6- μm microparticles penetrated the dielectrophoretic barriers, and straightly moved along with the flow toward the channel end, as indicated by letter 'A'. On the other hand, the 16- μm beads behaved in a different way. They were deflected from the stream by the DEP barriers and slowly moved along the electrode edges (B). The particles moved toward the open end of the barrier and then reverted to the subsequent barrier. These two types of movements were observable only when a flow rate was carefully set between the threshold velocities of the two particles. In the test, the threshold velocities were experimentally found and then the working flow rate was determined. It was found that the experimental threshold velocities were close to those obtained from the numerical model (Chen et al. 2006). The flow rate was readily set and programmed through the keypad of the syringe pump.

4.2 Particle separation

The motion trajectories of particles discussed in Sect. 4.1 gives rise to possible approaches of particles separation, by taking advantages of their differences in traveling distances or traveling velocities. The scheme of separation with the present electrode system has been discussed in Sect. 2 (Fig. 1b). In this section, experimental tests were carried out with the 9.6 and 16 μm microbeads. The process of separation is shown in Fig. 7. The particle suspension was first introduced into the channel with a low flow rate of $\sim 100 \mu\text{m/s}$ (below the threshold velocity), while the electrodes were energized with a voltage of $15 V_{pk-pk}$. As the particles approached the first electrode pair, they were accumulated and aligned there due to the low flow velocity (Fig. 7a). This electrode pair of a 90° aligning angle served as an accumulator where all the particles lined up for the subsequent operation. Particle aggregation was partially

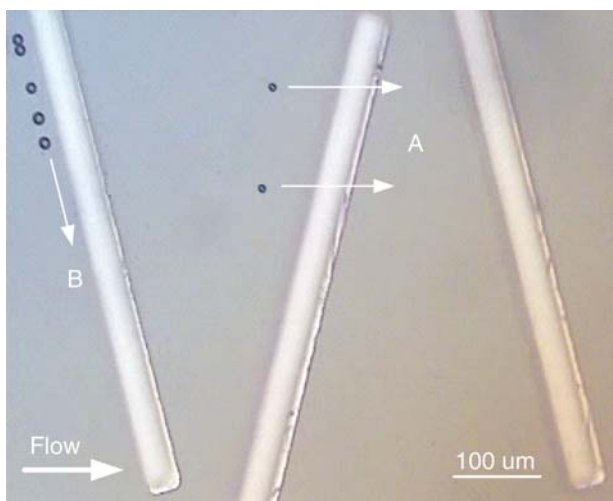
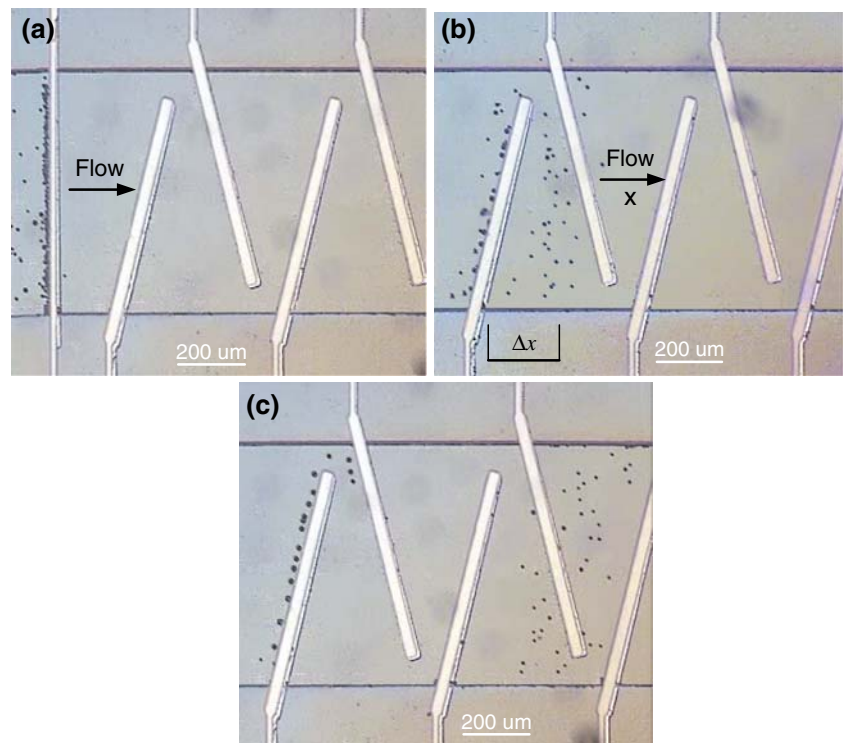


Fig. 6 Trajectories of particle movements when a flow of region II (Fig. 2) is applied from left to right. **a** The smaller particles of 9.6 μm penetrated the DEP barriers and moved along with the flow. **b** The larger particles of 16 μm were deflected by the DEP barriers and moved along the electrode edges. The aligning angle of the electrodes was 75° and the applied voltage was $15 V_{pk-pk}$ at 1 MHz

Fig. 7 Separation of the 9.6 and 16 μm spheres. The aligning angle of the electrodes was 75° and the applied voltage was $15 V_{\text{pk-pk}}$ of 1 MHz. The flow rate was $90 \mu\text{l/h}$ (mean flow velocity $\sim 400 \mu\text{m/s}$). **a** Accumulation of the particle mixture near the fluidic inlet. **b** The released particles followed the two different paths and separation occurred at the electrode pairs. **c** After 1.5 s from **b**, the distance between the two separated subpopulations increased



observed at this stage due to the particle interactions. However, the aggregate would break down as the voltage was turned off.

Following the accumulation step, the particles were then released from the accumulator by switching its voltage off (but voltage on other electrodes is still on) and increasing the flow rate to the working domain, which was in between the threshold velocities of the two particles (Region II). The released particles moved along the flow, and separation occurred once they reached the electrode pairs, as shown in Fig. 7b. The mean flow velocity was $\sim 400 \mu\text{m/s}$ in this case. The 16 μm moved along the electrode edges with a very low speed while the 9.6 μm directly penetrated the electrode pairs and moved along with the flow at a constant speed ($\sim 400 \mu\text{m/s}$). This resulted in the spatial separation of the two particles. The two subpopulations of particles traveled at different velocities and became more and more separated as they moved further along the channel (Fig. 7c). As expected, the 16- μm beads snaked their way along the electrodes, while the 9.6 μm ones moved straightly toward the end of the channel. A long channel would be an advantage in this application. In this case, a channel of 10 mm covered with electrode was used.

The separation distance between the two particles is plotted as a function of time in Fig. 8. The analytical values were calculated from $\delta x = V_0(1 - \cos^2 \theta)\delta t$, with Δx being the distance in flow direction. The

experimental values were measured from the clips captured by a CCD video camera. The clips were analyzed frame by frame with reference to the time indicated by the software. Distances were measured by comparing with the marks (with known positions) defined at several locations at the microfabrication stage. Measurements were taken with individual particles and averaged values were used in the plot. Two flow velocities, i.e., 348 and 496 $\mu\text{m/s}$, were studied in the test. In general, the experimental results agreed well with the analytical calculations. Separation distance increased linearly and rapidly with time. Further more, the separation was significantly observable in a very short time. For example, the distance between the two separated particles was $\sim 3.0 \text{ mm}$ within 10 s at the flow velocity of 348 $\mu\text{m/s}$. This rapid processing time would be beneficial to practical applications.

The separated subpopulations of particles would reach the outlet of the channel subsequently in time. The 9.6 μm particles first arrived there and the 16 μm particles arrived at a later time. This allowed a time interval for the operation of collection. To examine this process, the number of particles that passed by the inspection window was counted as a function of time (Fig. 9). The inspection window was located close to the outlet and counts were taken by examining the video clip. Two distinct peaks representing the two particles were observed at the time of ~ 18 and ~ 110 s after the releasing, respectively. In the test, a channel

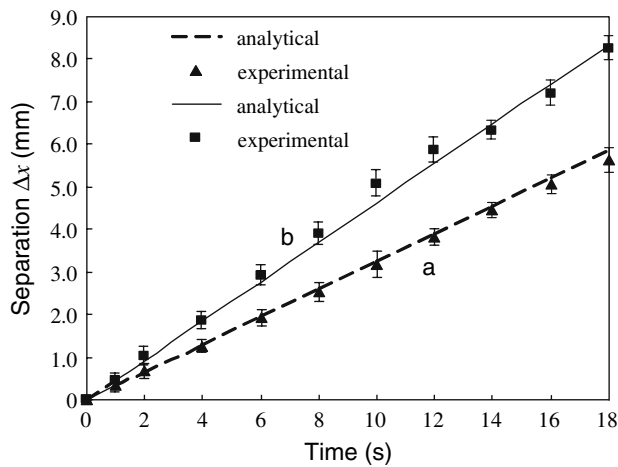


Fig. 8 Spatial separation distances in flow direction (indicated with x , Fig. 7b) of the 9.6 and 16 μm particles versus time. Shown are two cases of flow velocities: **a** 348 $\mu\text{m}/\text{s}$ and **b** 496 $\mu\text{m}/\text{s}$. Both analytical and experimental values are plotted for each case. The voltage applied was 15 $V_{\text{pk-pk}}$ and the frequency was 1 MHz

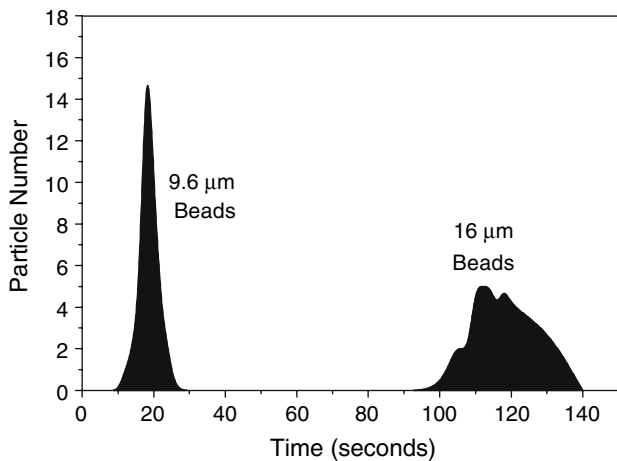


Fig. 9 Fractionation of the 9.6 and 16 μm beads. Particle counts were plotted as a function of time at the inspection location (close to channel outlet). The two *peaks* represented the separation in time space of the two particles

of 10 mm long was used. In such a channel, the two subpopulations were separated by a time interval of >1 min. The particles would be more separated in time if a longer channel (with electrodes) is used.

4.3 Discussion

The feasibility of separating particles of the present microfluidic system has been demonstrated mainly with a typical design. The basic specifications of this design are: the aligning angle of the electrodes was 75° and the electrode width was 40 μm ; the channel width was 800 μm and length (with electrodes) was 10 mm; the channel height was 75 μm , etc. These parameters

highly influence the performance of the system, and an optimization process of the parameters is of importance to improve the performance of the system. This would be a topic of future work. On the other hand, the particles were separated based on their different sizes in this paper. In fact, the system is also capable of separating particles of same size but of different electrical properties.

5 Conclusion

A dielectrophoretic barrier-based microfluidic device for separation of micro-sized particles has been presented. This work takes advantage of the flow rates within the medium region for the purpose of particle separation. The 3D electrode configuration overcomes the problems encountered in the planar electrodes such as particle adhesion at walls. The particles running along with the flow may follow different trajectories at different velocities with a proper arrangement of the parameters, resulting in the separation of the particles. The two subpopulations of particles were separated into observable distances in a rapid time (tens of second). The separated subpopulations reached the outlet at a sufficiently long interval, which was beneficial to the subsequent operation such as particle collection.

References

- Chen DF, Du H, Li WH (2006) A 3D paired microelectrode array for accumulation and separation of microparticles. *J Micromech Microeng* 16:1162–1169
- Chen DF, Du H, Li WH (2005) Numerical modeling of dielectrophoresis using a meshless approach. *J Micromech Microeng* 15:1040–1048
- Dürr M, Kentsch J, Müller T, Schnelle T, Stelzle M (2003) Microdevices for manipulation and accumulation of micro- and nanoparticles by dielectrophoresis. *Electrophoresis* 24:722–731
- Huang Y, Pethig R (1991) Electrode design for negative dielectrophoresis. *Meas Sci Technol* 2:1142–1146
- Hughes MP, Morgan H, Rixon FJ, Burt JPH, Pethig R (1998) Manipulation of herpes simplex virus type 1 by dielectrophoresis. *BBA-Gen Subjects* 1425(1):119–126
- Jones TB (1995) *Electromechanics of particles*. Cambridge University Press, Cambridge, New York
- Kralj JG, Lis MTW, Schmidt MA, Jensen KF (2006) Continuous dielectrophoretic size-based particle sorting. *Anal Chem* 78:5019–5025
- Li HB, Bashir R (2002) Dielectrophoretic separation and manipulation of live and heat-treated cells of *Listeria* on microfabricated devices with interdigitated electrodes. *Sens Actuators B Chem* 86:215–221
- Pethig R (1996) Dielectrophoresis: using inhomogeneous AC electrical fields to separate and manipulate cells. *Crit Rev Biotechnol* 16(4):331–348

- Pethig R, Huang Y, Wang XB, Burt JPH (1992) Positive and negative dielectrophoretic collection of colloidal particles using interdigitated castellated microelectrodes. *J Phys D Appl Phys* 25:881–888
- Pohl HA (1978) *Dielectrophoresis*. Cambridge University Press, Cambridge, New York
- Schnell T, Müller T, Gradl G, Shirley SG, Fuhr G (1999) Paired microelectrode system: dielectrophoretic particle sorting and force calibration. *J Electrostat* 47:121–132
- Schnelle T, Müller T, Reichle C, Fuhr G (2000) Combined dielectrophoretic field cages and laser tweezers for electro-tation. *Appl Phys B* 70:267–274
- Washizu MO, Kurosawa, Arai I, Suzuki S, Shimamoto N (1995) Applications of electrostatic stretch-and-positioning of DNA. *IEEE Trans Ind Appl* 31(3):447–456